Sedimentary Geology 341 (2016) 13–26

Contents lists available at ScienceDirect

Sedimentary Geology

journal homepage: www.elsevier.com/locate/sedgeo

Influence of deposit architecture on intrastratal deformation, slope deposits of the Tres Pasos Formation, Chile

Neal C. Auchter [a], Brian W. Romans [a], Stephen M. Hubbard [b]

[a] Department of Geosciences, Virginia Polytechnic Institute and State University, Blacksburg, VA 24061, United States
[b] Department of Geoscience, University of Calgary, Calgary, AB T2N 1N4

ARTICLE INFO

Article history:
Received 26 January 2016
Received in revised form 4 May 2016
Accepted 4 May 2016
Available online 20 May 2016

Editor: B. Jones

Keywords:
Intrastratal deformation
Depositional architecture
Submarine landslide
Detachment plane
Mass transport deposit (MTD)
Slope deposits

ABSTRACT

Slope sediments on passive and active margins deform and fail across a broad range of scales ranging from loading and sediment remobilization near the sediment–water interface to submarine landslides and mass movements that incorporate significant volumes of slope deposits. Deformational styles are characterized by updip extension and downdip compressional features that occur above a detachment surface. Conditions for failure and deformation include the presence of weak layer(s) that serve as a detachment surface, competency contrasts that allow for detachment and downslope movement, deformation above a detachment surface, and a triggering mechanism(s) that initiates failure. Slope failure processes and products are well documented at scales resolvable by seismic-reflection surveys and in instances of extensive downslope failure, but the processes and products associated with intermediate-scale slope deformation are poorly understood.

Intrastratal deformation is defined as stratigraphically isolated zones of deformation bounded above and below by concordant and undeformed strata. In this study, outcrop examples of intrastratal deformation from the Upper Cretaceous Tres Pasos Formation are used to elucidate the influence of depositional architecture on slope deformation. The facies distribution associated with compensational stacking of lobe deposits is shown to have a first-order control on the location and style of deformation. Detachment planes that form in mudstone deposits associated with lobe fringe and interlobe deposits are spatially limited and deformation is restricted to interbedded sandstone and mudstone associated with off-axial lobe positions. Downslope translation was arrested by stratigraphic buttresses associated with more sandstone-prone axial deposits. Emplacement of a regionally extensive mass transport deposit is interpreted as the triggering mechanism for contemporaneous intrastratal deformation of >60 m of underlying stratigraphy. A vertical increase in ductile deformation through the deformation interval indicates the role of burial depth and compaction. Distinguishing synburial intrastratal deformation (10s of m below seafloor) from tectonic or at-seafloor deformation has important implications for interpretations of burial history, slope stability, and potential triggering mechanisms.

1. Introduction

Slope sediments on both passive and active margins deform and fail across a broad range of scales ranging from soft sediment deformation and sediment remobilization near the sediment water interface (Butler et al., 2015) to submarine landslides and mass movements associated with detachment surfaces that occur deeper below the seafloor (Hampton et al., 1996; Frey-Martínez et al., 2006; Moscardelli and Wood, 2008, 2015; Sharman et al., 2015). As much as 80% of mass failures occur within 100 m of the seafloor (Devore and Sawyer, 2016), indicating a general threshold of shear strength within that interval, above which sediment more readily deforms and fails in response to stress. Previous studies concerned with slope failure processes and products have largely focused on seismic-reflection-scale examples, which have highlighted the development of weak layers and detachment surfaces (Hampton et al., 1996; Perret et al., 1995; Locat et al., 2014), mechanisms associated with failure and deformation along the slope (Frey-Martínez et al., 2006; van der Merwe et al., 2009; Devore and Sawyer, 2016), and the morphometry of resulting deposits and their impacts on subsequent slope sedimentation (Armitage et al., 2009; Jackson and Johnson, 2009; Olafiranye et al., 2013; Kneller et al., 2015; Moscardelli and Wood, 2015). However, due to limits in resolution, these studies are unable to identify smaller-scale (bed-scale to 100s of m) deformational features associated with slope mass movement and are preferentially skewed toward examples where the distance of movement is significant (i.e., evacuation, translation, and deformation resulting in slides and slumps). Moreover, few studies have focused on aspects of sediment deformation where failure was arrested prior to significant downslope movement (i.e., 'failed slides' sensu Frey-Martínez et al., 2006). Here, we consider the stratigraphic product of intrastratal deformation that was not associated with continued failure and submarine landslide development. Intrastratal deformation is defined as stratigraphically isolated zones of deformation bounded above and below by concordant and undeformed strata

http://dx.doi.org/10.1016/j.sedgeo.2016.05.005
0037-0738/

(c.f. Conglio, 1986). We emphasize the influence of depositional architecture on the location and scale of intrastratal deformation; as such, we document an early phase of landslide development, evidence for which is commonly eradicated by subsequent failure and deformation.

We posit that evidence for pre-mass failure processes are nuanced in the stratigraphic record, recorded by evidence for intrastratal deformation at the sub-seismic scale. This study focuses on outcrop examples of intrastratal deformation recorded in turbiditic slope deposits of the Upper Cretaceous Tres Pasos Formation, Magallanes Basin, southern Chile. We consider depositional processes and architecture, development of weak layers in buried sediment, and the role of mass-transport deposit (MTD) emplacement to better understand the nature and geologic implications of intrastratal deformation. Primary objectives are to: (1) document the scale, orientation, and style (i.e. extension vs. compression) of intrastratal deformation features at the meter to kilometer scale; and (2) investigate the relative influence of 3D depositional architecture and shear-strength variations within a stratigraphic succession on intrastratal deformation.

1.1. Conditions for detachment surfaces

An important factor in the development of gravity-influenced detachment planes is the presence of weak layers. The term 'weak layer' refers to a stratigraphic layer consisting of sediment or rock that has an actual or potential strength that is significantly lower than adjacent stratigraphic layers; the resulting competency contrast provides a potential focus for the development of a detachment surface (sensu stricto Locat et al., 2014). Weak layers can occur at nearly any scale as long as the appropriate conditions are met. The competency contrasts that produce weak layers can result from a number of factors including lithology (Cartwright, 2011), clay content, grain size, depth and rate of burial (Williams, 1960; Lewis, 1971; Day-Stirrat et al., 2013), and diagenetic processes during burial (Perret et al., 1995; Cartwright, 2011). Development of a detachment surface at a weak layer is further influenced by the slope of deposited sediment, amount and configuration of pore space, pore pressure, and changes in effective normal stress induced by rapid burial, seismic shaking, storm wave or tsunami impact, or rapid removal of overburden (Williams, 1960; Lewis, 1971; L'Heureux et al., 2012; Kvalstad et al., 2005; Locat et al., 2014; Cardona et al., 2016). Locat et al. (2014) provide a review of sediment types and the main effects influencing weak layers associated with submarine slides. While these factors and triggering mechanisms for induced weak layers are commonly considered for large-scale mass movements, they are less commonly applied at the scale of outcrops.

1.2. Mass transport deposits

Mass transport deposits (MTDs) result from gravity-driven mass failure and downslope movement of previously deposited material (Dott, 1963; Nardin et al., 1979; Moscardelli and Wood, 2015). These deposits encompass a range of geometries and internal characteristics associated with limited downslope mass movement of slumps and slides with correspondingly minor internal deformation, to significant downslope movement of rafted blocks and debris flows, recording complete evacuation from the failure position. Such mass-wasting processes result in some of the largest sedimentary deposits on Earth (Haflidason et al., 2005; Kvalstad et al., 2005; Lamarche et al., 2008). The volume of a single MTD can range from several m^3 to over 5500 m^3 and areal coverage can be greater than 35,000 km^3 (Kneller et al., 2015; Moscardelli and Wood, 2015). Mass transport deposits are typically characterized by topographically complex and laterally variable bounding surfaces. The surfaces and margins of MTDs can include headwall scarps, extensional ridges and blocks, discrete lateral margins, basal ramps and flats, remnant blocks, translated and/or rotated blocks, rafted blocks, pressure ridges, and fold-thrust systems, all of which contribute to variable surface topography (Moscardelli et al., 2006; Moscardelli and Wood, 2008; Bull et al., 2009; Alves, 2010). Subsequent deposition of sediment gravity flows over variable MTD topography can result in significant lateral variability in stratigraphic architecture and facies distribution. Outcrop examples of turbiditic packages thinning onto as well as scouring into underlying MTDs have been previously documented in the Tres Pasos Formation (Armitage et al., 2009; Romans et al., 2009) and have been reviewed by Kneller et al. (2015). Armitage et al. (2009) proposed that the stratigraphic architecture of overlying lobe and/or channel deposits is driven or influenced by inherited MTD topography. However, the influence of MTD emplacement and MTD-driven stratigraphic architecture on intrastratal deformation has not been addressed.

2. Geologic background

Studies in the Magallanes Basin (48–53° S) of southern Chile spanning the past four decades have provided a robust and growing suite of sedimentologic, stratigraphic, structural, and geochronologic data (e.g., Winn and Dott, 1977; Wilson, 1991; Fildani and Hessler, 2005; Shultz and Hubbard, 2005; Hubbard et al., 2010, 2014; Armitage et al., 2009; Covault et al., 2009; Romans et al., 2009, 2010; Fosdick et al., 2011; Bernhardt et al., 2012; Malkowski et al., 2015; Schwartz and Graham, 2015). Hubbard et al. (2010) demonstrated that progradation of a foredeep-axial slope system with ~1 km shelf-to-basin relief infilled the basin during the Late Cretaceous linked to relatively high-magnitude and long-lived foredeep subsidence. The Tres Pasos Formation represents the slope depositional system, which is genetically related to shallow-marine and deltaic deposits of the overlying Dorotea Formation (Fig. 1).

In the northern part of the Ultima Esperanza District, outcrops have been studied at Cerro Divisadero (Romans et al., 2009), Cerro Escondido (Covault et al., 2009), along the Rio Zamora at Cerro Cagual (Shultz et al., 2005), along the Rio de Las Chinas (Schwartz and Graham, 2015), and Sierra Contreras (Armitage et al., 2009) (Fig. 1A). Outcrops occur along generally east-dipping ridges with minor structural complications (e.g., local west-verging reverse faults with 10–50 m of offset and associated drag folds). In this region, Tres Pasos Formation stratigraphic thickness ranges from 1 to 1.5 km with stratigraphic architectures dominated by: (1) discordant mudstone-rich intervals interpreted as MTDs; (2) lenticular to tabular sandstone-rich bodies interbedded with concordant siltstone and mudstone packages interpreted as turbidite deposits; and (3) thick units of thin-bedded turbidites attributed to slope sedimentation lateral to major down-slope sediment-routing systems (Romans et al., 2011). Tide- and wave-influenced shallow-marine and fluvial deposits of the lowermost Dorotea Formation overlie the Tres Pasos Formation and are interpreted to represent a shelf-edge deltaic sequence (Covault et al., 2009; Schwartz and Graham, 2015). The prevalence of MTDs within the Tres Pasos succession suggests a depositional system in which slope failure was an important process that influenced deposition.

This study is restricted to outcrop exposures along the Rio Zamora valley at Cerro Cagual, which comprise heterolithic and sandstone-rich turbiditic deposits intercalated with MTDs (Fig. 2). The study area is focused along a ~1 km long by ~70 m thick depositional dip-parallel outcrop of almost 100% exposure, which is part of a ~3.5 km long transect along the Rio Zamora valley (Fig. 2).

3. Stratigraphic data and analysis

Stratigraphic data for the study area include 15 measured sections logged at cm-to-dm resolution along the 3.5 km Rio Zamora transect (Fig. 2B), with an additional series of sections logged at cm resolution (Fig. 3A). High-resolution photomosaics provide additional stratigraphic context and information about facies association transitions (e.g., Fig. 2C). Stratigraphic sections capture characteristic

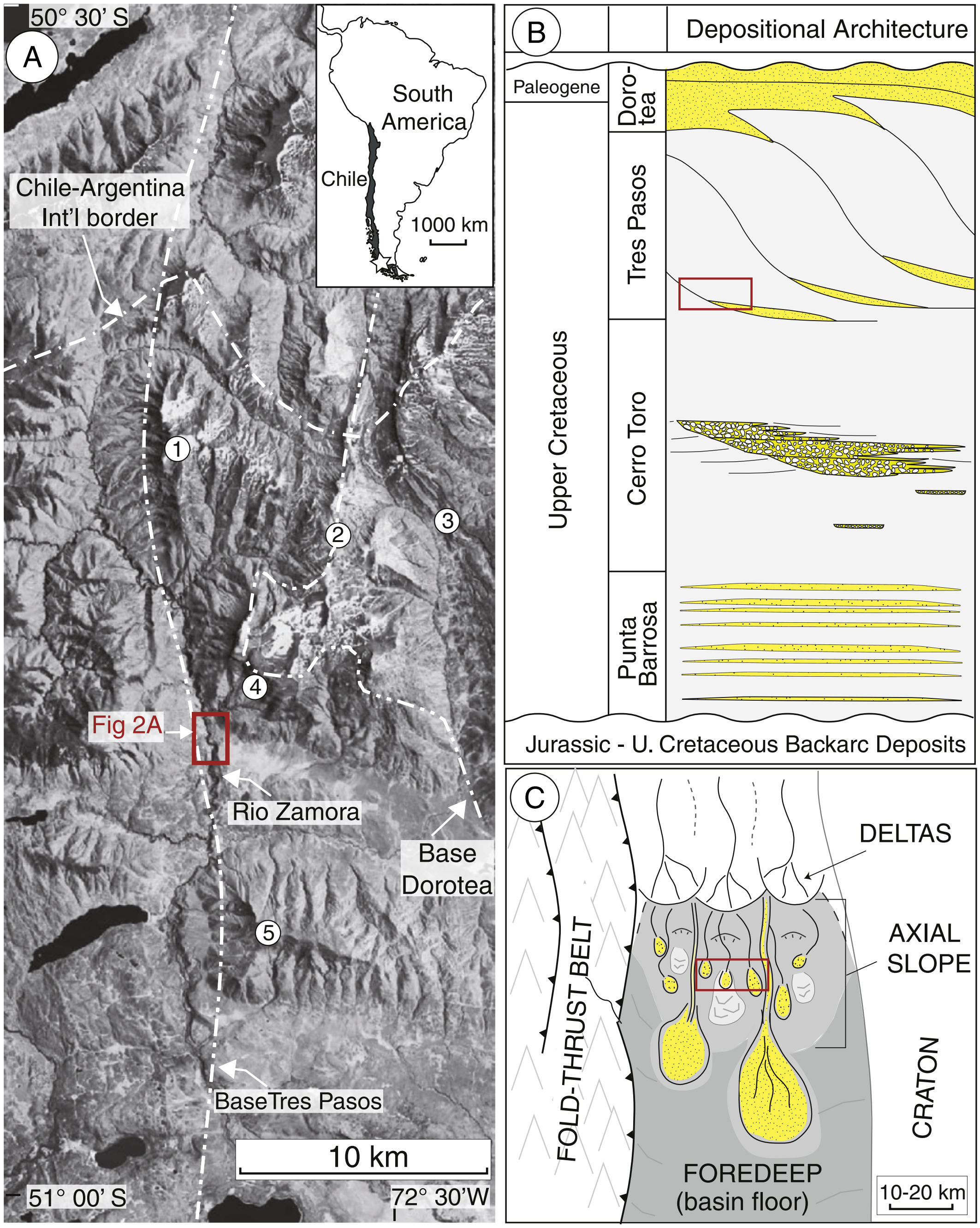

Fig. 1. Regional overview; red boxes show the approximate location of the study area. (A) Satellite image of the study region. Numbered locations are previous studies: (1) Cerro Divisadero (Romans et al., 2009); (2) Cerro Escondido (Covault et al., 2009); (3) Rio de las Chinas valley (Schwartz and Graham, 2015); (4) Cerro Mirador (now referred to as Cerro Cagual; Shultz et al., 2005); (5) Sierra Contreras (Armitage et al., 2009). The approximate basal contacts of the lithostratigraphically defined Tres Pasos and Dorotea Formations are shown with dashed lines. Inset shows the study region at the southern end of South America, denoted with a star. (B) Generalized stratigraphic column for the Magallanes foreland basin showing depositional architecture of the main stratigraphic units. The Punta Barrosa and Cerro Toro Formations were deposited in bathyal water depths; the Tres Pasos and Dorotea Formations were deposited at progressively shallower depths and record infilling of the deep-water seaway. (C) Simplified Cretaceous paleogeographic reconstruction of the Magallanes foreland basin showing a southward prograding slope filling the basin axially and parallel to the Andean orogenic front. Parts B and C modified from (Fildani et al., 2009). (For interpretation of the references to color in this figure legend, the reader is referred to the web version of this article.)

grain size, bed thickness, physical structures, and the nature of bedding contacts. Paleoflow was measured from flutes, grooves, and current parting lineations.

3.1. Sedimentary facies associations

Sedimentation units, lithological beds, and their internal sedimentary structures represent the fundamental order of observation. A sedimentation unit is interpreted to record all deposition that occurs from a single subaqueous sedimentary density flow (e.g., turbidity current, hyperconcentrated density flow, or debris flow; sensu Lowe (1982); see also Mulder and Alexander (2001); Talling et al. (2012)). Internal divisions and sedimentary structures are identified and described based on characteristics outlined by Bouma et al. (1962) and Lowe (1982). Beds of similar affinity are grouped as bedsets, which form the next hierarchical order of observation. Bedsets that can be mapped laterally at the outcrop scale (10s of meters) are grouped into distinct facies associations.

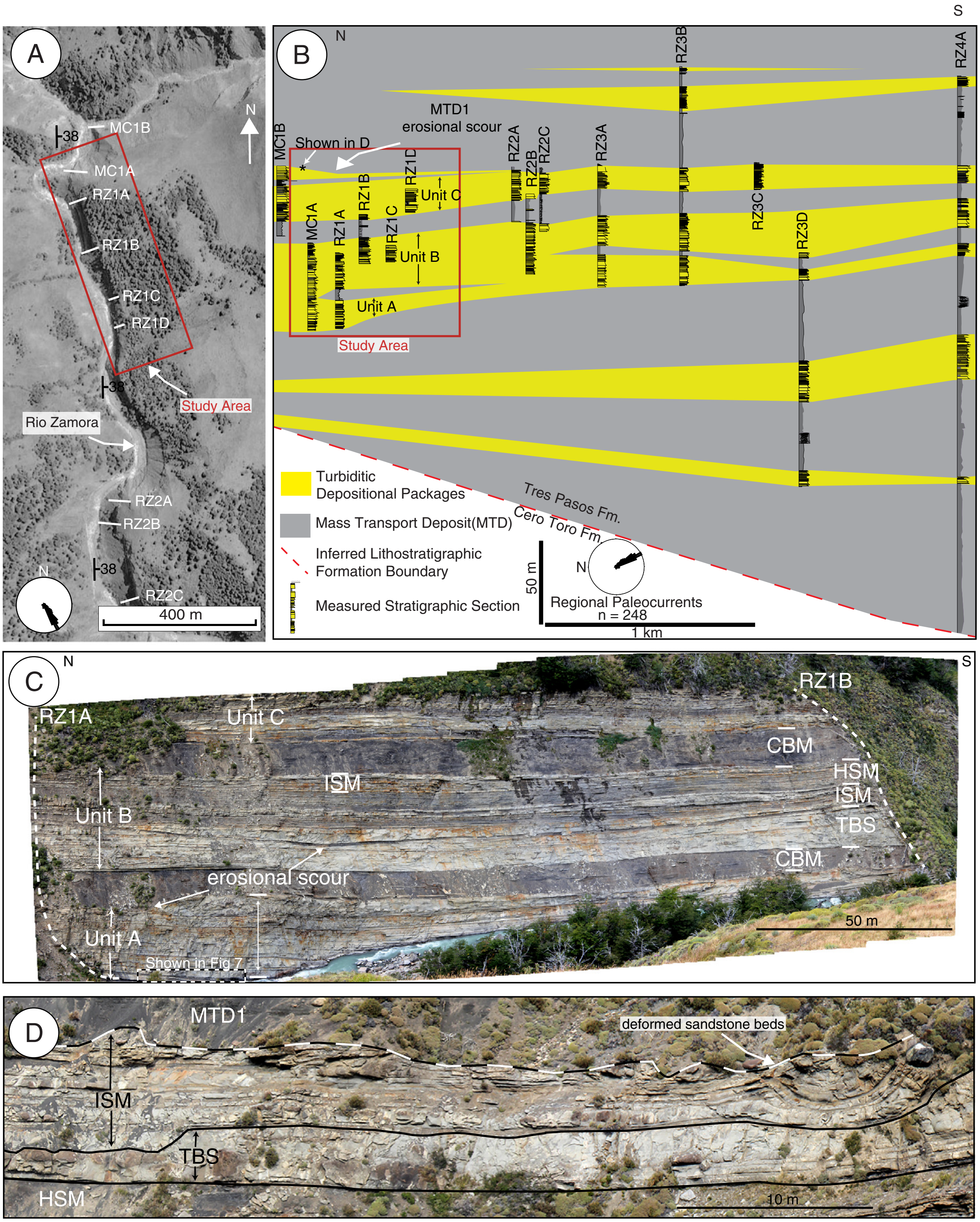

Fig. 2. (A) Satellite with the study area denoted by the red box. White lines indicate measured sections. Regional paleoflow measurements are dominantly to the south-southeast. Beds are dipping to the east as a result of uplift/tilting associated with eastward propagation of the Patagonian fold-thrust belt. (B) Correlation diagram for a 3.5 km transect along the Rio Zamora valley. Yellow indicates turbiditic packages and gray indicates MTDs. The study area is denoted with the red box. Depositional packages in the study area are labeled Units A, B, and C. Note the erosional scour from the regionally extensive MTD1 into the underlying strata above Unit C. (C) Representative outcrop along the Rio Zamora valley showing depositional packages (Units A, B, and C) and facies associations: thick-bedded sandstone (TBS), interbedded sandstone, siltstone, and mudstone (ISM), heterolithic thin-bedded siltstone and mudstone (HSM), and chaotically bedded mudstone (CBM). Inset shows the location of Fig. 7A. (D) Example of MTD plowing and deformation of underlying strata at the basal interface of MTD1. The depositional package is located north of section MC1A and is erosionally truncated to the south above Unit C. (For interpretation of the references to color in this figure legend, the reader is referred to the web version of this article.)

We subdivide the deposits of the Tres Pasos Formation into four sedimentary facies associations: (i) thick-bedded sandstone facies (TBS); (ii) interbedded sandstone, siltstone and mudstone facies (ISM); (iii) heterolithic thin-bedded facies (HSM); and (iv) chaotically bedded mudstone facies (CBM) (Table 1). Deposits are described in accordance with a stratigraphic approach wherein no a priori interpretation of depositional environment is applied at any hierarchical level.

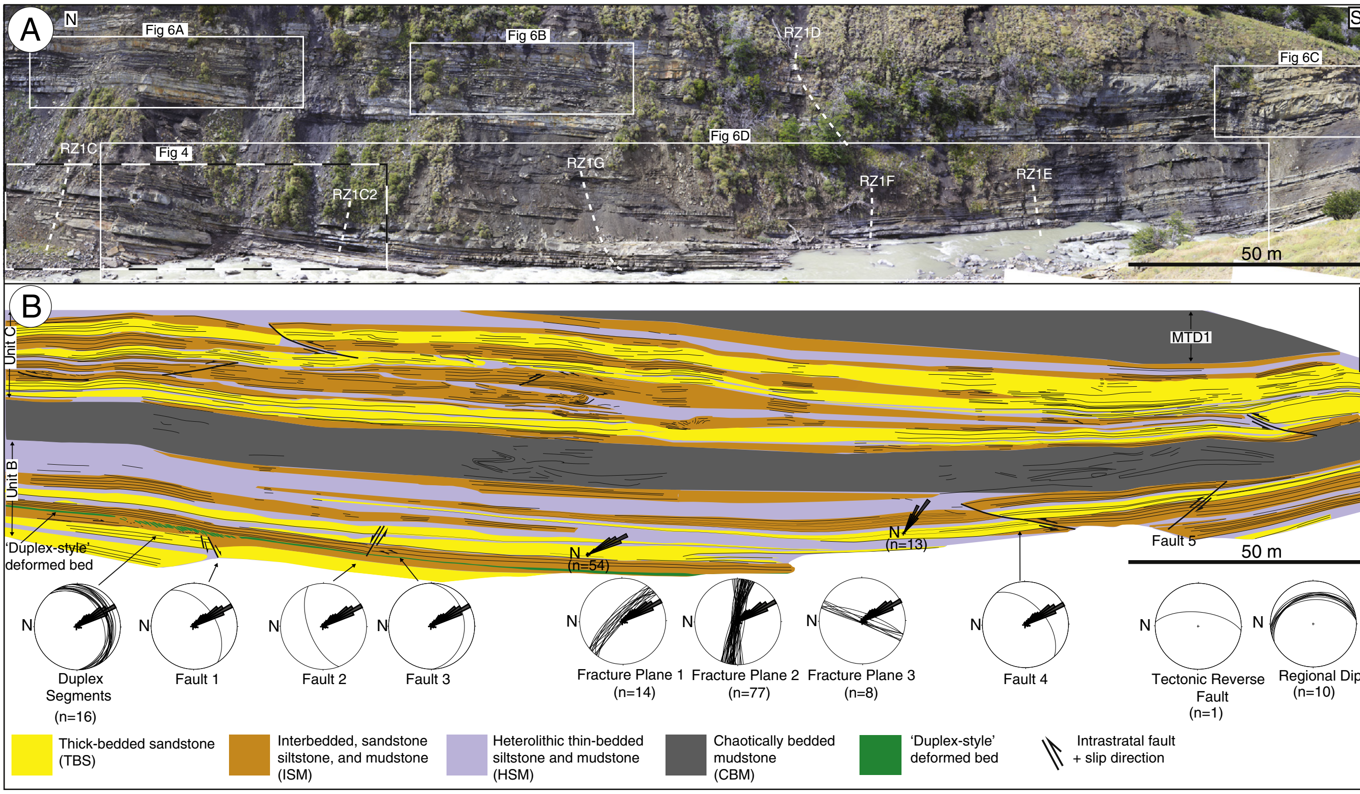

Fig. 3. (A) Photomosaic of the 350 m × 40 m primary focus area. Boxes show the locations of Fig. 4 and examples from Fig. 6. Dashed lines show the location of measured sections. (B) Interpreted line drawing of the mosaic shown in A. Colors represent facies associations explained in Table 1. Stereonets show the orientation of planar measurements and are superimposed on a rose diagram of regional paleocurrent measurements (n = 248). Fracture plane orientations were measured from concordant segments of the duplex-style bed shown in green and adjacent beds. Measurements from a tectonic reverse fault and regional strike and dip of strata are shown at far right. Rose diagrams overlain on bedsets in Unit A (n = 54 and n = 13) demonstrate changes in paleoflow direction between bedsets. Note: north in stereonets is rotated to left to align with outcrop perspective. (For interpretation of the references to color in this figure legend, the reader is referred to the web version of this article.)

3.2. Stratigraphic framework and general depositional model

Intervals of turbiditic deposits bound above and below by widespread MTDs are referred to as packages. Packages range in thickness from 10 to 60 m and can be mapped continuously along the transect at the multi-kilometer scale (>3.5 km). Packages comprise multiple genetically related bedsets, which are commonly composed of multiple facies associations. Bedsets are separated by stratigraphic surfaces,

Table 1
Description of facie associations, Tres Pasos Formation, Rio Zamora Valley at Cerro Cagual.

Facies associations	Dominant grain-size	Sedimentary structures	Turbidite divisions*	Bounding surfaces	Thickness	Secondary features	Depositional processes	Interpretation
Thick-bedded sandstone (TBS)	Fine to lower medium-grained sandstone	Normally graded; structureless or plane-laminated and/or ripple laminated; amalgamation of beds	S3/Ta-c	Sharp, undulating, or erosional base; gradational or sharp top	Sed units 30–200 cm	Laterally discontinuous basal mudstone intraclasts (<10 cm)	Rapid sedimentation from high density turbidity currents; traction and suspension sedimentation from low-concentration turbidity currents	Axial to off-axial lobe deposits
Interbedded sandstone, siltstone, and mudstone (ISM)	Fine-grained sandstone; siltstone; mudstone	Normaly graded; planar to ripple laminated sandstone; structureless or faintly laminated siltstone	Tb-e	Sharp or undulating base; sharp top	Sed units 5–30 cm	beds significantly thicken and thin laterally across 10s of meters	Traction and suspension sedimentation from low-concentration turbidity currents; hemipelagic settling	Off-axis to fringe lobe deposits
Heterolithic thin-bedded siltstone and mudstone (HSM)	Siltstone; mudstone	Normally graded; ripple to faint planar laminations	Tc-e	Sharp base; sharp top	Bed sets 15–200 cm; sed units <1–5 cm	Thin (<5 cm) lower fine to very fine-grained sandstone beds rare	Hemipelagic settling; suspension settling from dilute turbidity currents	Distal lobe fringe and interlobe deposits
Chaotically bedded mudstone (CBM)	Dominantly siltstone and mudstone; sandstone rare	Dominantly discordant to chaotic; some soft-sediment deformation; laterally discontinuous parallel lamination	-	Sharp, discordant, locally erosional base; sharp or variable top	Variable: 3–>50 m	Rafted blocks of silstone and/or sandstone	Mass wasting (slumps/slides); cohesive freezing of matrix-supported debris flows	Mass trasport deposits (MTDs): variable topography at tops of individual deposits

* 'S' divisions are from Lowe (1982); 'T' divisions are from Bouma (1962).

including laterally continuous mudstone horizons and low-relief erosional scours. Bedsets are dominantly tabular where composed of TBS, and are tabular to wedge-shaped where composed of ISM and HSM. Lateral changes in facies association and bedset thickness, in some instances thinning to termination (e.g., no traceable beds), are observed throughout the study area (Figs 3A). Facies association transitions and lateral bed thickness changes also reveal laterally offset, or compensational, stacking of bedsets (sensu Mutti and Sonnino, 1981; Deptuck et al., 2008; Prélat et al., 2009). The constructional nature of bedsets (i.e., lack of mappable erosional surface), lateral thinning despite the lack of evidence for significant erosional scour, and compensational stacking support an interpretation of lobe deposits for the MTD-bounded packages within the study area (Mutti and Sonnino, 1981; Deptuck et al., 2008; Prélat et al., 2009). The sedimentary bodies referred to here as lobes include zones of erosional scour, which suggest some degree of channelization. However, these zones are both rare in occurrence and minor in erosional relief (<3 m) in what are dominantly depositional geometries.

3.3. Local stratigraphic data and interpretation

Outcrop data was collected from the 70 m thick stratigraphic section that extends from the Rio Zamora upwards to the base of a regionally extensive (>150 m by >10 km in dip profile) MTD, referred to here as MTD1 (Fig. 2B). Strata are characterized by three ~15–20 m thick turbiditic packages separated by ~5 m thick MTDs. Unit A at the bottom of the interval is only exposed in the northern extent of the study area, and a depositional package above Unit C is locally eroded and deformed by MTD1 (Fig. 2D). The majority of field measurements focus on Units B and C due to field access. Units B and C are dominated by facies associations ISM and HSM, though TBS deposits are also present. Measurements record dominantly southeasterly paleoflow (mean of 150°; Fig. 2).

The areal extent of an individual lobe and the lateral shifting of successive lobes through time are fundamental controls on resulting stratigraphic architecture (Straub and Pyles, 2012). Similar to studies of submarine lobe systems from outcrop (e.g., Prélat et al., 2009) and seafloor/shallow subsurface datasets (e.g., Deptuck et al., 2008), we recognize lateral facies association transitions in Units B and C from thick-bedded sandstone (TBS), interpreted as lobe axis deposits, to interbedded sandstone and siltstone (ISM) off-axis deposits, to silt- and mudstone-prone (HSM) lobe fringe deposits. This axis-to-fringe transition occurs both in longitudinal and cross-sectional profiles with individual lobes stratigraphically separated from underlying and overlying lobes by widespread fine-grained deposits, or interlobe strata.

At larger spatial and temporal scales, and superimposed on lateral lobe switching, are progradational, aggradational, and retrogradational phases of lobe stacking (Prélat et al., 2009; Prélat and Hodgson, 2013). The net result is a 3D mosaic of the facies associations that transition laterally in a relatively predictable fashion (e.g., ISM transitions to HSM in one direction and TBS in the other) but change vertically in a less predictable fashion (e.g., HSM transitions to TBS). Facies association heterogeneity in Units B and C is interpreted to result from lobe depositional processes occurring over various spatial and temporal scales. The mechanical and rheological differences between the different facies associations, which are influenced by grain size, grain packing, clay content and compaction, have important implications for subsequent deformation.

4. Deformation data and analysis

Measurements of deformed strata include the orientation of fault planes, slickenlines, and fracture planes. Field measurements were used in combination with photomosaics and differential GPS to calculate the amount of offset on faults, to determine the amount of extension and shortening, and to provide stratigraphic context for deformational features. Planar measurements were restored and plotted on a stereonet (Allmendinger et al., 2011; Cardozo and Allmendinger, 2013). All measured fault planes are reported after correcting for regional tectonic deformation (350/38 E). Planes are restored to 0° and do not account for any dip that may have been associated with the paleoslope. Regional tectonic tilt is oriented eastward, therefore correctional rotation does not influence inferred paleoslope angle (i.e., southward).

Distinguishing between deformation associated with slope processes and tectonic deformation is inherently challenging in uplifted foreland basin deposits. In the Magallanes Basin, Cretaceous strata have been regionally tilted to the east as a result of post-Cretaceous propagation of the Patagonian fold-thrust belt in the Eocene through present (Wilson, 1991; Fosdick et al., 2013). Local deformation occurs in Tres Pasos Formation strata in the form of reverse faults and associated west-northwest verging drag folds. Regional tilting, associated backthrusting, and related fracture orientations have been identified and documented in the study area and are consistent with published structural interpretations for the Magallanes Basin (Wilson, 1991; Fosdick et al., 2011, 2013) (Fig. 3B). We distinguish intrastratal (synburial) from tectonic deformation features in this study area based primarily on the internally consistent fault orientation within intrastratal units, striking NNW–SSE prior to correction (mean strike of 030), and the close agreement between fault dip direction and regional paleoflow orientation (southeast). These orientations are distinct from regional, tectonically controlled faults that strike N–S (mean strike of 350). We also consider continuity and length scale of individual deformation features and the geometry of detachment surfaces (e.g. Waldron and Gagnon, 2011; Korneva et al., 2016).

4.1. Occurrence and style of deformation

Deformational features are bound above and below by undeformed, concordant strata and preferentially overlie discrete mudstone intervals (HSM). Dip directions of faults are generally oriented parallel to paleoslope based on alignment with paleoflow indicators. For clarification, we use the terms ‘downdip’ and ‘updip’ to refer to the relative position of features on a slope, and the terms ‘downslope’ and ‘upslope’ to refer to processes or movement in that direction.

Extensional features include normally faulted single beds, normally faulted bedsets that are offset as coherent blocks, and bed-scale boudinage. Measured fault plane orientations show displacement in a downdip direction (SE; e.g., Fault 1) and antithetically in an updip direction (NW; e.g., Fault 2) (Figs. 3, 4). Bed-scale boudinage is characterized by brecciated and isolated, or ‘floating,’ sandstone bed segments encased in ductilely deformed mudstone (Fig. 4C). Based on a pre-deformation line length the apparent extension across the interval of bed-scale boudinage is ~12 m.

Intrastratal compressional features comprise reverse faults including isolated faults or duplex-style thrusts separating imbricated bed segments, bedsets offset as coherent blocks, ductilely folded bedsets, and ductilely deformed mudstone deposits. Deformation is generally restricted to facies associations ISM and HSM. Bedsets faulted as coherent units are characterized by vertically displaced blocks with thrust faults at both their downdip and updip extent (e.g., Unit B; Fig. 3B).

There are two duplex-style deformed beds in Unit B (Fig. 4B; Beds 4 and 5), which are ~20–30 cm thick and interbedded with ~10–20 cm thick mudstone intervals (ISM) (Fig. 4). The upper of the two beds consists of 26 discrete imbricated bed segments bound by southeast-dipping reverse faults. Orientation of the imbricated fault planes, bed thickness at the updip ‘origin’, maximum thickness of each bed segment (typically at the center of the segment), the downdip ‘terminus’ thickness, bed segment length from origin to terminus, and the orientation of additional fracture planes on bed segments are summarized in Appendix A. In order to calculate shortening, each bed was measured at its center where it is assumed to be the original bed thickness of

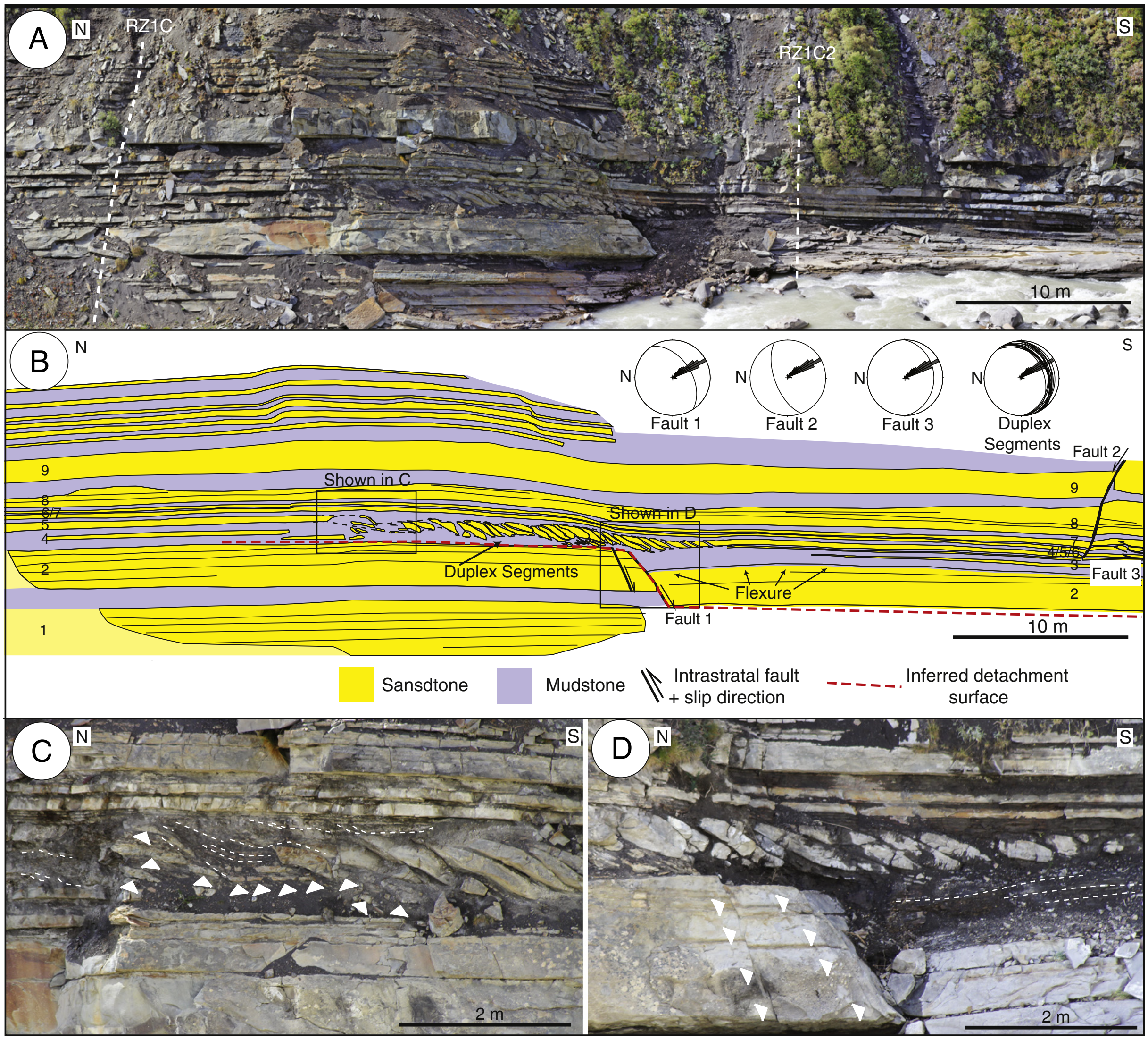

Fig. 4. (A) Outcrop from the inset box in Fig. 3A. (B) Interpreted line drawing of part A highlighting location and nature of intrastratal deformation features. Stereonets from Fig. 3B demonstrate that dip direction of measured fault planes are generally parallel with paleocurrent measurements. Insets show the location of C and D. Note: north in stereonets rotated to left to align with outcrop perspective. (C) Detailed view of intrastratal extensional features updip of compressional features within the same bed. Bed-scale boudinage is marked by white triangles. Ductilely deformed and folded HSM deposits above Bed 5 are highlighted with white dashed line. Note the abrupt transition from extensionally brecciated bed segments to duplex-style compression with thrust direction as up depositional dip. (D) Detailed view of duplex-style compression of a single sandstone bed directly overlying extensionally faulted thick-bedded sandstone. White triangles mark fault surfaces. Dashed white line highlights deformed HSM. (For interpretation of the references to color in this figure legend, the reader is referred to the web version of this article.)

~26 cm based on measurements from the concordant positions of the bed adjacent to the deformational zone. The bed segment was then marked at the updip and downdip extent where the bed thickness was half of the central 'full' bed thickness. Bed segments were then restored based on measured half thicknesses to account for overlap and deformational thinning. The length of duplex-style deformation is 21 m and the sum of all measured segments is 33 m, which results in 12 m of apparent shortening. Shortening is balanced by ~12 m of apparent extension at the north (updip) end of the deformational zone characterized by boudinage and ductile deformation of HSM deposits (Fig. 4).

4.2. Timing of deformation

Based on observations and arguments discussed above, a tectonic origin for the observed deformation features is unlikely. In the context of deformation related to the depositional slope, two hypotheses for the depth and timing of deformation are considered: (1) deformational features formed below the seafloor in buried sediment as a result of a single event, and (2) deformational features that occurred at the seafloor and, thus, at differing times upwards through the succession. Here we review depositional patterns and architecture, and their association with deformational features, in order to evaluate these competing interpretations. Detailed examples are drawn from bed-scale observations in Unit B, as well as qualitative observations from the succession as a whole. Beds and genetically related bedsets in Unit B are numbered in Fig. 4B for reference.

The first set of observations addresses a 33 m long zone of deformation in Unit B that influences Beds 4 and 5 above and to the north of Fault 1 (Fig. 4A, B). Duplex-style deformation of Beds 4 and 5 are generally uniform in style, with dips to the southeast. This interval is evidence for the prevalence of ductile deformation, particularly apparent in HSM deposits surrounding Beds 4 and 5 (Fig. 4C). HSM deposits underlying Bed 5 are ductilely deformed and compacted into subtle mounds (black dashed line Fig. 4B). HSM deposits above Bed 5 are characterized by folded and chaotically deformed laminae. Additionally, Bed 5 segments change orientation and degree of overlap above mounded HSM deposits and grade into more regularly oriented segments from north to south (Fig. 4B). These observations indicate that deformation of Beds 4 and 5 was concomitant or occurred sequentially at different times under very similar stress conditions. Similarly, ductile deformation of deposits overlying Bed 5 indicates that either existing HSM deposits deformed commensurate with Bed 5 or were deposited after deformation of Bed 5 and then subsequently deformed. We find a single deformational event to be most parsimonious.

A second set of observations focuses on beds extensionally offset by Fault 2. Fault 2 offsets Beds 5–9 to the northwest with ~10 cm of vertical throw (Fig. 4B). Within that set of beds, Bed 8 is erosionally truncated and was therefore deposited and eroded prior to faulting (Fig. 4B). Based on these stratigraphic relationships, either Beds 5–9 were faulted at the same time, or Fault 2 is a progressive growth fault with each bed offset sequentially. A growth interpretation predicts beds will thicken above the hanging wall on the downthrown side of a normal fault in response to increased accommodation at the seafloor. Due to the uniform offset of all beds and lack of appreciable thickness change for any bed across Fault 2, we interpret Fault 2 to have slipped during a single event that offset Beds 5–9 contemporaneously.

A third set of observations focuses on bed-scale folding and depositional thinning associated with Fault 1. Bed 2 is extensionally offset by Fault 1 with ~1 m of vertical throw (Fig. 4). On the hanging wall of Fault 1, Bed 2 preserves subtle folding characterized by convex-up flexure extending from Fault 1 to Fault 2 (Fig. 4B). Preserved flexure indicates Bed 2 was sufficiently consolidated to sustain and preserve ductile strain associated with vertical displacement of the Fault 1 hanging wall. Additionally, below Fault 2, Bed 3 thins from south to north toward Fault 1 and is not identified at section RZ1C where it has thinned into facies association IHS (Fig. 4B). Bed thinning toward Fault 1 is not consistent with a growth fault interpretation, which would predict the opposite. Bed thinning is consistent with the observation of bed-scale compensational stacking observed throughout the study area.

Combining these lines of evidence we interpret Fault 1 to be a localized bend in a more extensive detachment surface (red dashed line, Fig. 4B) and that all deformation in Unit B is related to movement along that detachment. The bend at Fault 1, where it crosses and offsets Bed 2, produces a steepening bend above Bed 2 and a flattening bend below Bed 2 (Figs. 4B, 5B). Bedding above a convex-up fault surface is predicted to lengthen and bend in order to accommodate the space problem created by the steepening bend during extension and downward vertical offset (Figs. 4B, 5B) (Xiao and Suppe, 1992; Patton, 2005). Brittle rupture and duplex-style stacking of bed segments bound by reverse faults antithetic to Fault 1 may be caused by continued extension over a steepening fault surface (Patton, 2005) and/or interaction with a downdip buttress that causes backthrusting (Vendeville, 2005).

Bedding above a concave-up surface is expected to fold downward to accommodate the space created by extension and may include brittle fracturing along the fold hinge (Xiao and Suppe, 1992). This is consistent with flexure of Bed 2 and the location of Fault 2 (Fig. 4A, B), which is antithetic to Fault 1 and generally projects to the hinge of Bed 2 flexure. Due to this internal consistency and the uniform offset of beds 5–9 by Fault 2, we interpret all deformation associated with Faults 1 and 2 to be contemporaneous and reject the growth fault hypothesis. Considering all of Unit B, we find that calculated apparent shortening above Fault 1 (~12 m) is comparable with calculated shortening further south at Faults 4 and 5 (~11 m) (Figs. 3, 4). We therefore interpret all deformational features in Unit B to be kinematically linked.

Broadening our scope of observation, we consider deformation from all depositional packages within the study area. Comparing duplex-style deformation in Unit A (Fig. 7A, B) with that of Unit B (Fig. 4) and Unit C (Fig. 7C, D, E), there is a qualitative increase in ductile deformation of sandstone beds upwards through the three stratigraphic units. Imbricate bed segments of Unit A are separated by little or no mudstone and bed segments are generally more tabular and isopachous than in Unit B. On the other hand, deformed beds in Unit C are notably more folded than in Unit B (Fig. 7E). These observations indicate that deformation in discrete depositional packages occurred under potentially different rheological conditions. The collection of observations supports the interpretation that deformation occurred below the seafloor and sufficiently precludes an interpretation that deformation occurred at or near the seafloor. We consider all deformation from Units A, B, and C to have occurred at the same time in response to a single triggering event. Based on measured stratigraphic thicknesses and depth below MTD1 we estimate burial depths for each unit to be ~60–70 m (Unit A), ~30–40 m (Unit B), and ~10 m (Unit C). It is unclear how much strata was erosionally removed during deposition of MTD1.

4.3. Conceptual model for intrastratal deformation

Intrastratal deformation at Rio Zamora is interpreted to have occurred via load-induced shear failure triggered by MTD emplacement along multiple detachment planes within the underlying strata. We describe a three-phase model for (1) triggering, (2) failure, and (3) cessation of downslope readjustment. These phases are illustrated in Fig. 5, which is a conceptualized evolution to account for deposits of Unit B, where linked extensional and compressional elements of downslope failure are observed.

4.3.1. Phase 1: triggering via MTD emplacement

We interpret that the emplacement of the regionally extensive MTD1 above Unit C (Fig. 2) was the trigger for intrastratal deformation. Downslope transport and emplacement of MTDs can occur nearly instantaneously following catastrophic failures of slope and shelf deposits (Maslin et al., 2005), imparting a significant increase in lithostatic (normal) stress and shear stress in the direction of transport on underlying strata (van der Merwe et al., 2009). We interpret that MTD1 (thickness > 150 m) emplacement induced a significant increase in normal stress; the plowing and erosion of underlying strata (Fig. 2D) indicates significant shear stress at the interface with the basal MTD surface.

The impacts of rapid emplacement of significant lithostatic load on underlying strata include rapid compaction and dewatering, which can cause abrupt changes in effective stress, liquefaction and/or thixotropic behavior of silt- and clay-rich layers, and development of overpressured layers (Williams, 1960; Lewis, 1971). These effects on underlying slope strata can create conditions appropriate for the development of detachment surfaces.

4.3.2. Phase 2: failure along detachment surfaces

Weak layers that develop into detachment surfaces are relatively laterally continuous (10s to 100s of meters) and occur in stratal stacking patterns that produce significant vertical competency contrasts (e.g., HSM interbedded with TBS). The lateral continuity of weak layers is a function of depositional architecture and is therefore predicted to preferentially occur in distal lobe and/or interlobe facies (HSM), where high aspect ratio bedsets are expected (e.g., Prélat et al., 2009). Similarly, vertical juxtaposition of lower competency HSM deposits and higher competency sandstone-prone packages of ISM or TBS due to compensational stacking of depositional elements can create a situation ideal for development of detachment surfaces.

Rapid deposition of silt and fine sand from sediment gravity flows can result in loose packing, relatively high pore-fluid volume, and relatively low shear strength (Williams, 1960). Rapid loading of stratigraphically confined layers of loosely packed silt is consistent with MTD emplacement, and can reduce the volume of the layer, resulting in increased neutral stress (pore-fluid) and decreased effective stress (grain-to-grain contact). Liquefaction can occur if these become equal, at which point the buried intrastratal layer behaves as a concentrated suspension and flows downslope. Upon cessation of flow, the layer returns to solid state (Williams, 1960).

Another potential mechanism for failure along a detachment surface is related to clay fabrics in fine-grained layers. The platy nature of clay

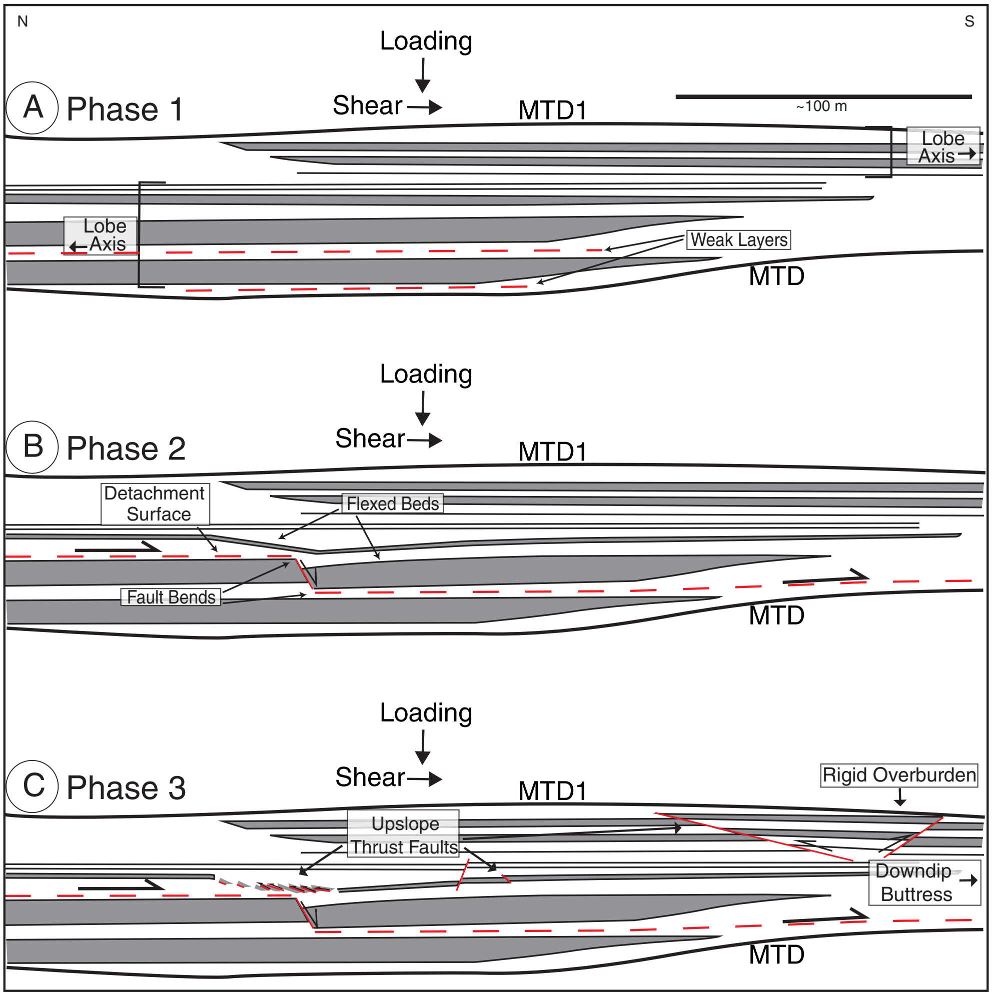

Fig. 5. Multi-phase interpretation for intrastratal deformation based on Unit B (Figs 3, 4). (A) Phase 1: Deposition of MTD1 produces increased lithostatic load and shear stress from downslope movement and interaction with the seafloor. The locations of weak layers in fine-grained deposits (white) are highlighted between sandstone-prone deposits (gray). Bedsets of a lower and upper lobe show compensational stacking (axes to the north and south respectively). Note MTD1 is not directly above Unit B, but Unit C is not shown here in order to highlight the deformational evolution of Unit B. (B) Phase 2: development of a detachment surface along weak layers. Downslope extension above the detachment surface induces ductile deformation in overlying strata. (C) Phase 3: Arrested detachment as mobile strata abuts a downslope stratigraphic buttress. The higher shear strength of axial lobe deposits, and underthrusting from downslope movement above the detachment plane result in upslope backthrusts. Rigid overburden from the MTD overlying Unit B may also limit vertical displacement.

minerals and their propensity to form flocs results in high porosity and disorganized mineral orientation when deposited by turbidity currents and hemipelagic fallout. Such layers can retain relatively high porosities through rapid burial resulting in overpressurization of pore fluids (Morley and Guerin, 1996; Morley, 2003, 2015). Overpressurization lowers shear strength, which can result in ductile flow and shearing. Shearing in high porosity clay-rich sediment has been shown to cause porosity loss and development of clay platelet alignment generally parallel to concordant strata (Day-Stirrat et al., 2013; Cardona et al., 2016). The development of a preferred orientation is interpreted to facilitate continued slip along that plane of weakness, thus creating a positive feedback resulting in shear failure along the plane of preferred orientation (Cardona et al., 2016). Detachment surfaces are interpreted to occur in HSM deposits overlying and/or interbedded with TBS deposits (Figs. 4, 6) via one or both of these mechanisms, as they are not mutually exclusive.

4.3.3. Phase 3: arrested detachment due to stratigraphic heterogeneity

Strata directly overlying detachment surfaces are interpreted to fail in a downslope direction due to the combined forces of gravity and shear stress from the emplaced MTD1. Failure is manifested as extensional faults, folds, and bed-scale boudinage at the updip end of a given detachment surface (e.g., Fault 1; Fig. 4B,C), and compressional faults, folds and contorted bedding at the downdip end (e.g., Fault 4; Figs. 4B, 7E). These updip and downdip deformation zones are consistent with submarine landslides and mass movements (Frey-Martínez et al., 2006; Moscardelli and Wood, 2008). However, an additional element documented in this study is the prevalence of upslope-directed deformation, and particularly upslope thrusts.

We interpret upslope-directed deformation to reflect the limited spatial extent of detachment planes and 3D heterogeneity associated with compensationally stacked bedsets. Lateral transition and vertical juxtaposition with more competent ISM and TBS facies associations resulted in spatial termination of the detachment surface. Therefore, translation above a detachment surface abutted downdip deposits that acted as a stratigraphic buttress. The buried nature of the strata in combination with underthrusting of the translated strata resulted in vertical displacement and upslope backthrusting in addition to downslope thrusts.

5. Discussion

5.1. Depositional influences on intrastratal deformation

5.1.1. Scale and extent of detachment surfaces

We propose that depositional architecture provides a first-order control on the scale and spatial distribution of downslope intrastratal

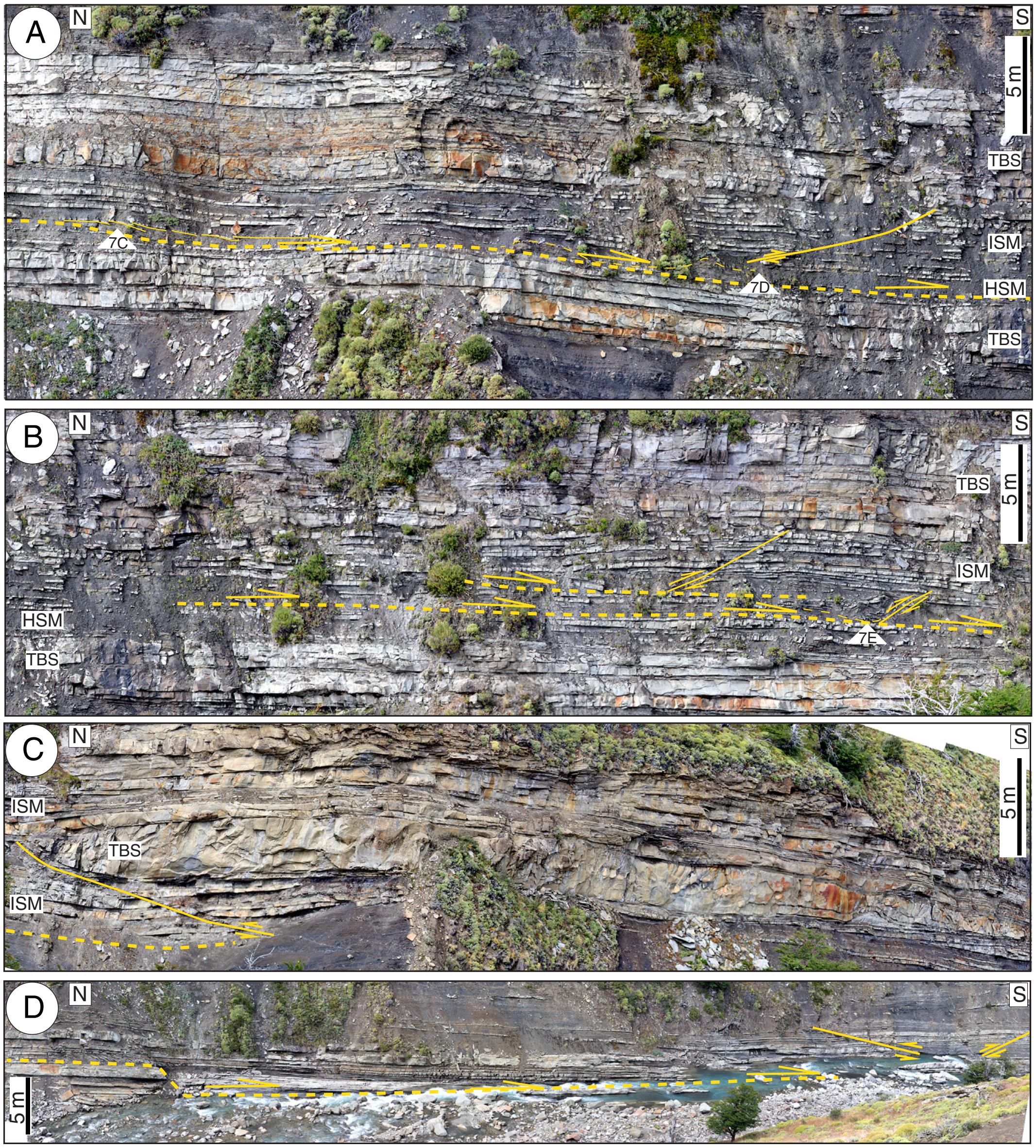

Fig. 6. Examples of detachment planes and overlying intrastratal deformation. Refer to Fig. 3 for locations and context. (A) Coherent slab of vertically displaced ISM deposits in Unit B. Offset includes a downslope thrust fault at the southern end of the slab and an upslope backthrust at the northern (updip) end of the slab. (B) Additional examples of downslope thrust faults in Unit B downdip of 6A. (C) Upslope backthrust of ISM and TBS deposits in Unit B downdip of 6B. (D) Full view of Unit A with interpreted detachment plane linking the updip extensional domain (Zone 1, Fig. 5C) to the downdip compressional domain (Zone 3, Fig 5C). (For interpretation of the references to color in this figure legend, the reader is referred to the web version of this article.)

deformation. The development of weak layers that have potential to become detachment surfaces requires deposition of sediment with relatively low shear strength such as mudstone, and vertical competency contrast with bounding layers of relatively high shear strength such as sandstone (Dott, 1963; L'Heureux et al., 2012; Locat et al., 2014). Sediment rheology can be further influenced by compaction and depth of burial at the time of failure (Alves, 2010; Chang et al., 2014; Sultan et al., 2007). In a lobe depositional setting, low-competency mudstone-prone deposits occur in lobe fringe and interlobe positions whereas high-competency deposits occur in more sandstone-prone lobe axis positions (Fig. 8). The 2D extent and 1D length of potential detachment surfaces in longitudinal profile are therefore directly linked to both the scale and stacking patterns of sedimentary bodies. For example, the lobes documented in this study are interpreted to have relatively limited areal extent due to underlying MTD topography (i.e., localized ponding; e.g., Armitage et al., 2009; Jackson and Johnson, 2009). However, a global compilation of outcrop and subsurface data by Prélat et al. (2010) demonstrate that lobes of similar volume vary in depositional area and thickness as a function of larger-scale confinement. The length-scales of detachment planes are therefore also predicted to scale with the lobe system in response to confinement and inherited topography.

5.1.2. Facies and stacking pattern control on stratigraphic buttresses

Lateral facies changes associated with depositional architecture (e.g., lobe axis-to-fringe transition) are also predicted to influence where intrastratal deformation is localized. Sandstone-prone axis deposits (TBS), mudstone-prone fringe deposits and interlobe intervals (HSM) have little internal heterogeneity and can be regarded as relatively uniform high and low shear-strength zones, respectively. Off-axis positions, where interbedded sandstone and mudstone beds have variable thickness (ISM), may have potentially more variable 2D shear strength. This variability in 2D shear strength associated with lateral facies changes, combined with compensational stacking of lobe

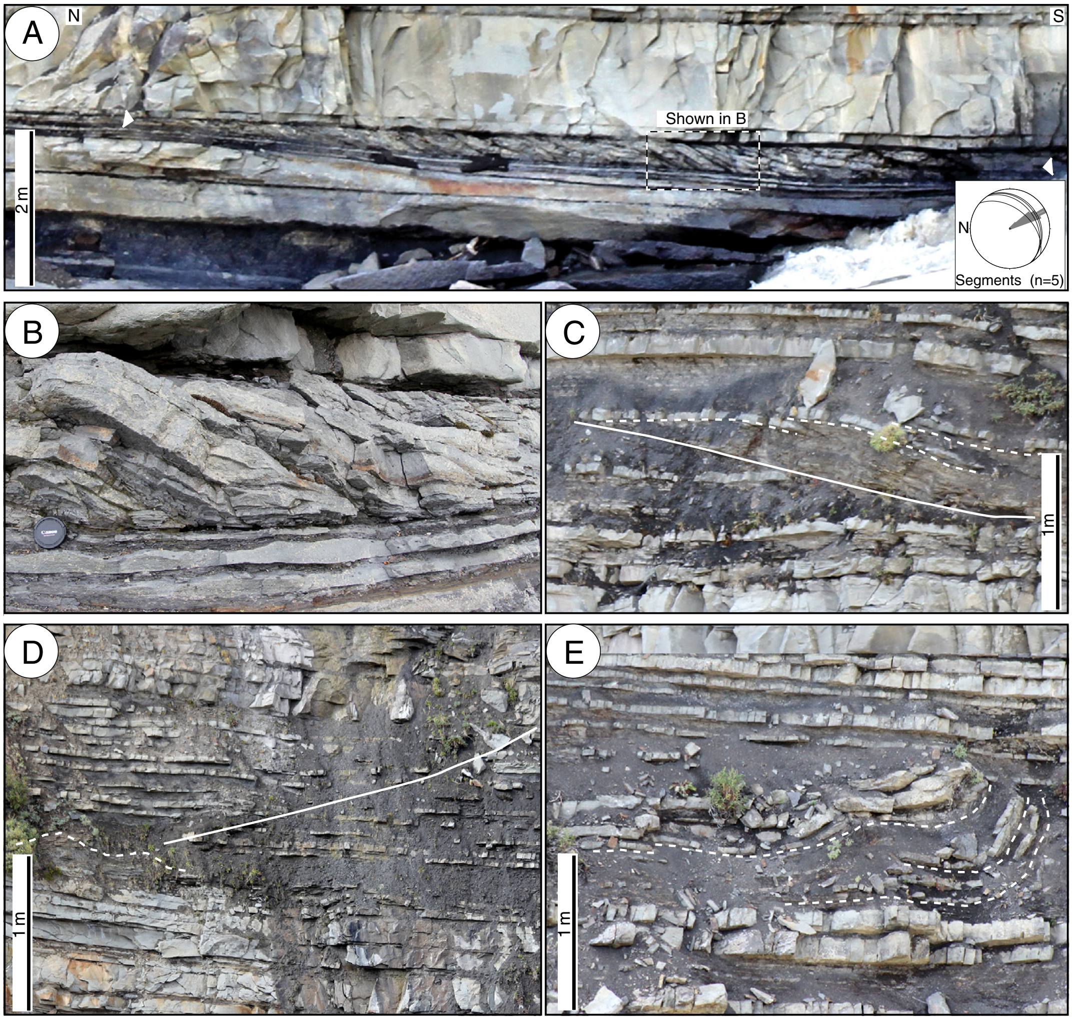

Fig. 7. Detailed examples of intrastratal deformation (locations for C–E are shown in Fig. 3). (A) Duplex-style bed segments bounded by northwest verging thrust faults near the base of Unit A. White triangles show the updip (N) and downdip (S) limits of deformation. (B) Bed segments from the bed shown in A (lens cap for scale). (C) Extensional deformation from Unit C characterized by ductile folding of ISM deposits with localized upslope backthrusts. (D) Compressional deformation from Unit C characterized by ductile mounding of HSM deposits and brittle downslope thrusting of ISM deposits. (E) Ductile folding and downslope compression of ISM deposits south of example D. (For interpretation of the references to color in this figure legend, the reader is referred to the web version of this article.)

elements, produces a 3D matrix of shear-strength heterogeneity (i.e., Unit C, Figs. 3, 6A, B). The result is stratigraphic buttresses characterized by high and low shear-strength elements that are laterally and/or vertically juxtaposed. Intrastratal deformation is predicted to occur in lithologically heterogeneous deposits (ISM) that translate downslope above detachment surfaces (HSM). Downslope translation is subsequently arrested where stratigraphic buttresses are encountered (Fig. 8B, C).

The geometry and deformational features in the Tres Pasos Formation bear important similarities to those documented in submarine landslides; namely, zones of updip extension and downdip compression above a detachment surface. Frey-Martínez et al. (2006) discuss stratigraphic factors that may contribute to the development of frontally confined, or buttressed, landslides with minimal downslope translation. We consider many of the intrastratal deformation features from the Tres Pasos Formation to be geometrically and kinematically analogous to frontally confined landslides with important differences in scale and confinement. The limited downslope translation above detachment surfaces (e.g., ~12 m) in the Tres Pasos Formation example may: (1) be appropriate for the limited length of the architecturally restricted detachment surface and/or; (2) reflect the influence in stratigraphic buttresses wherein the potential energy loss associated with detachment is lower that the potential energy required to overcome the downslope lobe axis barrier (Fig. 8).

5.2. Recognition of intrastratal deformation

Multiple studies have addressed the differences and distinguishing characteristics between soft-sediment versus tectonic deformation (e.g., Elliott and Williams, 1988; Waldron and Gagnon, 2011; Korneva et al., 2016). Criteria generally stipulate that soft-sediment deformation may be achieved via grain-level rearrangement of sediment, 'superficial' detachment planes that intersect the seafloor, and/or ductile folding of sandstone beds. In contrast, a 'rooted' décollement associated with a shear zone at depth and broad regional extent indicates tectonic deformation. These criteria illustrate the fundamental difference between the two: that soft-sediment deformation necessarily relates to a depositional system whereas tectonic deformation does not. Many scales of deformation fall within this broad application of soft-sediment deformation, ranging from bed-scale deformation and sediment remobilization within the kinematic boundary layer at or near the seafloor (Butler et al., 2015) to submarine landslides and mass movements that influence strata 10s of meters below the seafloor (Frey-Martínez et al., 2006; Lamarche et al., 2008; Moscardelli and Wood, 2008, 2015).

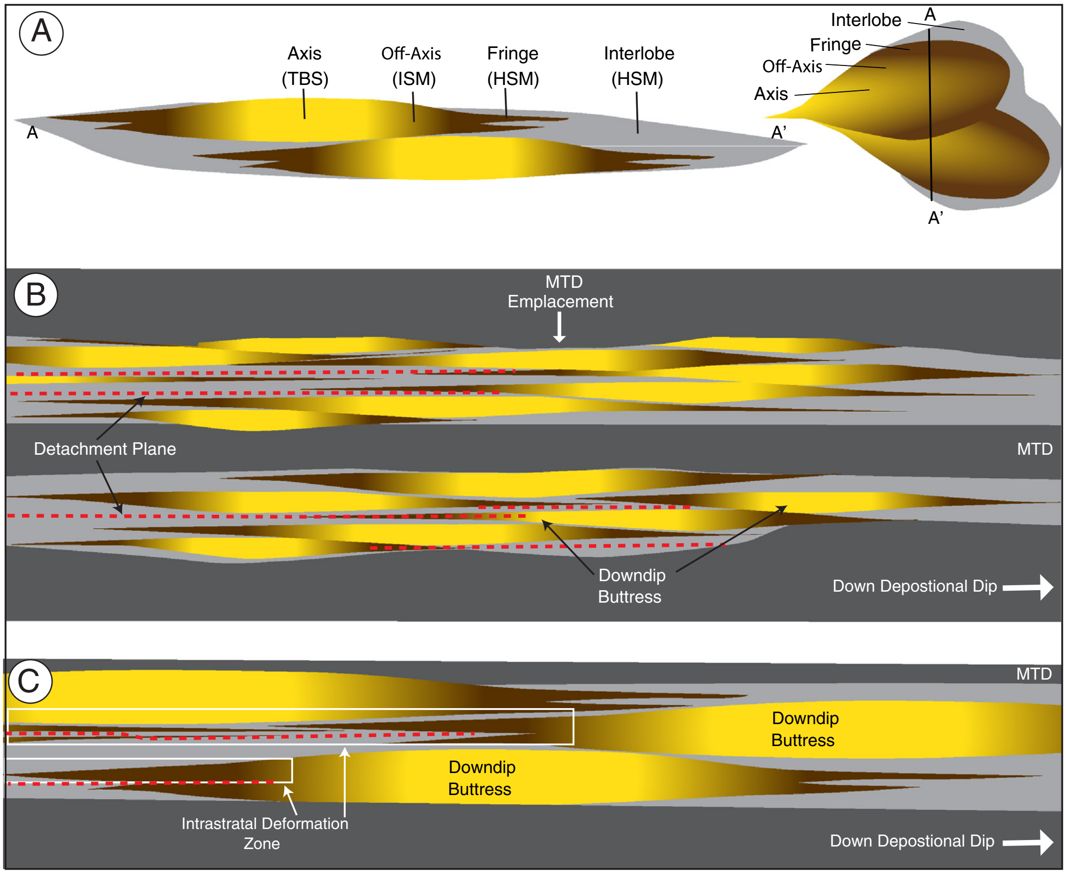

Fig. 8. Conceptual model illustrating how depositional architecture influences the occurrence and style of intrastratal deformation. (A) Simplified illustrations of compensationally stacked lobes in cross sectional and plan view showing fundamental facies association transitions from lobe axis to lobe fringe and interlobe. (B) Conceptual example of compensationally stacked lobes in dip profile. Sand-prone axial deposits function as downdip buttresses where underlying detachment planes terminate. (C) Higher-resolution conceptual example showing locations of potential detachment planes and associated intrastratal deformation zones. Detachment planes may form in intralobe positions within fine-grained deposits and/or interlobe deposits. Deformation is restricted to less competent fringe and off-axis deposits. (For interpretation of the references to color in this figure legend, the reader is referred to the web version of this article.)

The intrastratal deformation presented in this study includes features characteristic of both large- and small-scale end member examples (i.e., ductile folding of individual sandstone beds and downslope movement and deformation of bedsets above detachment surfaces). Placing this suite of deformational features on the spectrum of soft-sediment deformation, however, is non-trivial. An intrastratal deformation interpretation linking all deformational features to a single event or triggering mechanism is significantly different than interpreting each example as having deformed at the seafloor (Figs. 5, 8). The intrastratal interpretation provides insight into aspects of sediment loading and slope stability that have regional or basin-wide implications. An 'at seafloor' interpretation, however, necessarily entails that deformational zones in different stratigraphic levels are sequential, as each must have occurred at the seafloor along with sediment accumulation. We interpret deformation from the Tres Pasos Formation to have occurred after burial and leverage our findings to provide insight for distinguishing linked intrastratal deformation from deformation at or near the seafloor.

One stratigraphic relationship that supports an interpretation of intrastratal deformation is the presence and nature of concordant strata overlying deformational zones. Undeformed strata will lack thickness changes or lapout geometries, which indicate deposition was influenced by deformational topography. For example, there should be no stratigraphic growth associated with extensional faults. Another important stratigraphic relationship is abrupt lateral transitions between concordant strata and deformational zones of the equivalent bed or bedset. Finally, the orientation of intrastratal deformation features should be generally with the inferred paleoslope.

Depositional architecture as a deformational control predicts that location of intrastratal deformation reflects the 3D stratal stacking patterns associated with the slope depositional system, which distinguishes intrastratal deformation from more through-going detachment planes that are present in some shale intervals or salt layers. While we demonstrate intrastratal deformation controlled by lobe depositional architecture, these relationships need not be restricted to lobes. Sinuous submarine channel complexes also produce heterogeneity associated with channel-margin transitions, as do longer term depositional architectures that form due to lateral channel migration and vertical aggradation throughout the evolution of a channel complex (c.f. McHargue et al., 2011; Bain and Hubbard, 2016). Based on outcrop observations and experimental results, Moretti et al. (2003) suggested that the competency contrast between channel axis and margin/levee deposits would promote the development of fractures and what they refer to as 'syn-sedimentary shear zones', which develop parallel to channel margins. We further speculate that channel meander bends where crevasse splays are common may also produce conditions favorable for intrastratal deformation in splay deposits because they juxtapose typically mudstone-prone overbank deposits with tabular, massive sandstone-prone splay deposits.

6. Conclusion

Intercalated turbidite and mass transport deposits (MTDs) of the Tres Pasos Formation, southern Chile, record examples of slope-parallel intrastratal deformation that are distinct from at-seafloor (soft sediment) deformation or regional tectonic deformation. Intrastratal deformation is defined as stratigraphically isolated zones of deformation bounded above and below by concordant and undeformed strata. Turbiditic strata are composed of mudstone, thinly interbedded sandstone and mudstone, and thick-bedded sandstone facies that are arranged as compensationally stacked lobe deposits. Intrastratal deformation within lobe deposits is interpreted to have occurred via load-induced shear failure triggered by MTD emplacement along multiple detachment planes. Detachment planes preferentially develop in discrete, fine-grained weak layers. The location and spatial extent of weak layers are a function of depositional architecture.

The compensational stacking of lobe deposits and associated facies distribution has a first-order control on the location and style of deformation. Detachment planes that form in mudstone deposits associated with lobe fringe and interlobe deposits are spatially limited and deformation is restricted to off-axis interbedded sandstone and mudstone. Downslope translation of strata above a detachment surface is arrested by stratigraphic buttresses, comprised of sandstone-prone lobe axis deposits. Upslope backthrusts within deformational zones are interpreted to result from spatial termination of the detachment plane and/or mobile strata underthrusting and abutting downslope stratigraphic buttresses such as lobe axis deposits. Deformed intervals bound above and below by undeformed units indicate shear strength variability within buried strata that reflect the 3D heterogeneity associated with depositional architecture and stacking patterns. A vertical increase in ductile deformation through the deformation interval indicates the role of burial depth and compaction on sediment rheology.

The occurrence, scale, style, and thickness of intrastratal deformation offer important insight into conditions and processes associated with slope failure, mass movements, and submarine landslides. Identification of intrastratal deformation has implications regarding sediment burial history, slope stability, and potential triggering mechanisms for slope failure.

Acknowledgments

Funding was generously provided to Chile Slope Systems Joint Industry Project (CSS JIP) by our sponsors: Chevron, ConocoPhillips, Statoil, Shell, BG Group, Marathon Oil, Talisman Energy, Anadarko, Hess, BP, BHP Billiton, Maersk, and Nexen. We thank students and affiliates of the CSS JIP for their help and support collecting data, including: Lisa Stright, Sebastian Kaempfe, Sarah Southern, Dan Niquet, Sarah Jancuska, Ben Daniels, Aaron Reimchen, Dan Hill, and Dallin Laycock. Valuable thoughts and observations were also provided by Zane Jobe, Joris Eggenhuisen, Allesandro Cantelli, Jesus Ochoa, Per Pedersen, Ken Eriksson, Ben Gill, and Rick Law. We thank Hotel Explora and Don Pepe Alarcón and the Alarcón family for allowing us access to outcrops in Chile. We also thank reviewers Lorena Moscardelli and Chris Jackson and editors of Sedimentary Geology for their help in honing the focus of this manuscript.

Appendix A. Supplementary data

Supplementary data to this article can be found online at http://dx.doi.org/10.1016/j.sedgeo.2016.05.005.

References

Allmendinger, R.W., Cardozo, N., Fisher, D.M., 2011. Structural geology algorithms: vectors and tensors. Cambridge University Press.

Alves, T.M., 2010. 3D seismic examples of differential compaction in mass-transport deposits and their effect on post-failure strata. Marine Geology 271, 212–224. http://dx.doi.org/10.1016/j.margeo.2010.02.014.

Armitage, D.A., Romans, B.W., Covault, J.A., Graham, S.A., 2009. The influence of mass-transport-deposit surface topography on the evolution of turbidite architecture: the Sierra Contreras, Tres Pasos Formation (Cretaceous), southern Chile. Journal of Sedimentary Research 79, 287–301. http://dx.doi.org/10.2110/jsr.2009.035.

Bain, H.A., Hubbard, S.M., 2016. Stratigraphic evolution of a long-lived submarine channel system in the Late Cretaceous Nanaimo Group, British Columbia, Canada. Sedimentary Geology 337, 113–132. http://dx.doi.org/10.1016/j.sedgeo.2016.03.010.

Bernhardt, A., Jobe, Z.R., Grove, M., Lowe, D.R., 2012. Palaeogeography and diachronous infill of an ancient deep-marine foreland basin, Upper Cretaceous Cerro Toro Formation, Magallanes Basin. Basin Research 24, 269–294. http://dx.doi.org/10.1111/j.1365-2117.2011.00528.x.

Bouma, A.H., 1962. Sedimentology of Some flysch deposits: a graphic approach to facies interpretation. Elsevier, Amsterdam.

Bull, S., Cartwright, J., Huuse, M., 2009. A review of kinematic indicators from mass-transport complexes using 3D seismic data. Marine and Petroleum Geology 26, 1132–1151. http://dx.doi.org/10.1016/j.marpetgeo.2008.09.011.

Butler, R.W.H., Eggenhuisen, J.T., Haughton, P., McCaffrey, W.D., 2015. Interpreting syndepositional sediment remobilization and deformation beneath submarine gravity flows; a kinematic boundary layer approach. Journal of the Geological Society of London 2014–150. http://dx.doi.org/10.1144/jgs2014-150.

Cardona, S., Wood, L.J., Day-stirrat, R.J., Moscardelli, L., 2016. Fabric development and pore-throat reduction in a mass-transport deposit in the Jubilee Gas Field, Eastern Gulf of Mexico: consequences for the sealing capacity of MTDs. In: Lamarche, G. (Ed.), In submarine mass movements and their consequences, advances in natural and technological hazards research, pp. 27–37 http://dx.doi.org/10.1007/978-3-319-20979-1.

Cardozo, N., Allmendinger, R.W., 2013. Spherical projections with OSXStereonet. Computational Geosciences 51, 193–205. http://dx.doi.org/10.1016/j.cageo.2012.07.021.

Cartwright, J., 2011. Diagenetically induced shear failure of fi ne-grained sediments and the development of polygonal fault systems. Marine and Petroleum Geology 28, 1593–1610. http://dx.doi.org/10.1016/j.marpetgeo.2011.06.004.

Chang, K.T., Ge, L., Lin, H.H., 2014. Slope creep behavior: observations and simulations. Environment and Earth Science 275–287 http://dx.doi.org/10.1007/s12665-014-3423-2.

Covault, J.A., Romans, B.W., Graham, S.A., 2009. Outcrop expression of a continental-margin-scale shelf-edge delta from the Cretaceous Magallanes Basin, Chile. Journal of Sedimentary Research 79, 523–539. http://dx.doi.org/10.2110/jsr.2009.053.

Conglio, M., 1986. Synsedimentary submarine slope failure and tectonic deformation in deep-water carbonates, Cow Head Group, western Newfoundland. Canadian Journal of Earth Sciences 23, 476–490.

Day-Stirrat, R.J., Flemings, P.B., You, Y., van der Pluijm, B.A., 2013. Modification of mudstone fabric and pore structure as a result of slope failure: Ursa Basin, Gulf of Mexico. Marine Geology 341, 58–67. http://dx.doi.org/10.1016/j.margeo.2013.05.003.

Deptuck, M.E., Piper, D.J.W., Savoye, B., Gervais, A., 2008. Dimensions and architecture of late Pleistocene submarine lobes off the northern margin of East Corsica. Sedimentology 55, 869–898. http://dx.doi.org/10.1111/j.1365-3091.2007.00926.x.

Devore, J.R., Sawyer, D.E., 2016. Shear strength of siliciclastic sediments from passive and active margins (0–100 m below seafloor): insights into seismic strengthening. In: Lamarche, G., et al. (Eds.), Submarine mass movements and their consequences, advances in natural and technological hazards research 41, pp. 173–180. http://dx.doi.org/10.1007/978-3-319-20979-1.

Dott, R.H., 1963. Dynamics of subaqueous gravity depositional processes. American Association of Petroleum Geologists Bulletin 47, 104–128. http://dx.doi.org/10.1306/BC743973-16BE-11D7-8645000102C1865D.

Elliott, C.G., Williams, P.F., 1988. Sediment slump structures: a review of diagnostic criteria and application to an example from Newfoundland. Journal of Structural Geology 10, 171–182.

Fildani, A., Hessler, A.M., 2005. Stratigraphic record across a retroarc basin inversion: Rocas Verdes–Magallanes Basin, Patagonian Andes, Chile. Geological Society of America Bulletin 117, 1596. http://dx.doi.org/10.1130/B25708.1.

Fildani, A., Hubbard, S.M., Romans, B.W., 2009. Stratigraphic evolution of deep-water architecture: examples of controls and depositional styles from the Magallanes Basin, southern Chile. 10. SEPM Field Trip Guidebook, southern Chile 73 pp.

Fosdick, J.C., Romans, B.W., Fildani, A., Bernhardt, A., Calderón, M., Graham, S.A., 2011. Kinematic evolution of the Patagonian retroarc fold-and-thrust belt and Magallanes foreland basin, Chile and Argentina, 51°30's. Bulletin Geological Society of America 123, 1679–1698. http://dx.doi.org/10.1130/B30242.1.

Fosdick, J.C., Grove, M., Hourigan, J.K., Caldero, M., 2013. Retroarc deformation and exhumation near the end of the Andes, southern Patagonia. Earth and Planetary Science Letters 361, 504–517. http://dx.doi.org/10.1016/j.epsl.2012.12.007.

Frey-Martínez, J., Cartwright, J., James, D., 2006. Frontally confined versus frontally emergent submarine landslides: a 3D seismic characterisation. Marine and Petroleum Geology 23, 585–604. http://dx.doi.org/10.1016/j.marpetgeo.2006.04.002.

Haflidason, H., Lien, R., Sejrup, H.P., Forsberg, C.F., Bryn, P., 2005. The dating and morphometry of the Storegga slide. Marine and Petroleum Geology 22, 123–136. http://dx.doi.org/10.1016/j.marpetgeo.2004.10.008.

Hampton, M.A., Lee, H.J., Locat, J., 1996. Submarine landslides. Reviews of Geophysics 34, 33–59.

Hubbard, S.M., Fildani, A., Romans, B.W., Covault, J.A., McHargue, T.R., 2010. High-relief slope clinoform development: insights from outcrop, Magallanes Basin, Chile. Journal of Sedimentary Research 80, 357–375. http://dx.doi.org/10.2110/jsr.2010.042.

Hubbard, S.M., Covault, J.A., Fildani, A., Romans, B.W., 2014. Sediment transfer and deposition in slope channels: deciphering the record of enigmatic deep-sea processes from outcrop. GSA Bulletin 857–871 http://dx.doi.org/10.1130/B30996.1.

Jackson, C.A.L., Johnson, H.D., 2009. Sustained turbidity currents and their interaction with debrite-related topography; Labuan Island, offshore NW Borneo, Malaysia. Sedimentary Geology 219, 77–96. http://dx.doi.org/10.1016/j.sedgeo.2009.04.008.

Kneller, B., Dykstra, M., Fairweather, L., Milana, J.P., 2015. Mass-transport and slope accommodation: implications for turbidite sandstone reservoirs. American Association of Petroleum Geologists Bulletin http://dx.doi.org/10.1306/09011514210.

Korneva, I., Tondi, E., Jablonska, D., Celma, C.D., Alsop, I., Agosta, F., 2016. Distinguishing tectonically- and gravity-driven synsedomentary deformation structures along the Apulian platform margin (Gargano promontory, southern Italy). Marine and Petroleum Geology http://dx.doi.org/10.1016/j.marpetgeo.2015.12.009.

Kvalstad, T.J., Andresen, L., Forsberg, C.F., Berg, K., Bryn, P., Wangen, M., 2005. The Storegga slide: evaluation of triggering sources and slide mechanics. Marine and Petroleum Geology 22, 245–256. http://dx.doi.org/10.1016/j.marpetgeo.2004.10.019.

L'Heureux, J., Longva, O., Steiner, A., Hansen, L., Vardy, M.E., Vanneste, M., Haflidason, H., Brendryen, J., Kvalstad, T.J., Forsberg, C.F., Chand, S., Kopf, A., 2012. Identification of weak layers and their role for the stability of slopes at Finneidfjord, Northern Norway. In: Yamada, Y., Kawamura, K., Ikehara, K., Ogawa, Y., Urgeles, R., Mosher, D.C., Chaytor, J., Strasser, M. (Eds.), Submarine mass movements and their consequences, advances in natural and technological hazards research, 31, pp. 321–330 http://dx.doi.org/10.1007/978-94-007-2162-3.

Lamarche, G., Joanne, C., Collot, J.-Y., 2008. Successive, large mass-transport deposits in the south Kermadec fore-arc basin, New Zealand: the Matakaoa Submarine Instability Complex. Geochemistry, Geophysics, Geosystems 9. http://dx.doi.org/10.1029/2007GC001843 (n/a–n/a).

Lewis, K.B., 1971. Slumping on a continental slope inclined at 1° - 4°. Sedimentology 16, 97–110.

Locat, J., Leroueil, S., Locat, A., Lee, H., 2014. Weak layers: their definition and classification from a geotechnical perspective. In: Krastel, S. (Ed.)Submarine mass movements and their consequences, advances in natural and technological hazards research 3–12 http://dx.doi.org/10.1007/978-3-319-00972-8.

Lowe, D.R., 1982. Sediment gravity flows: II. Depositional models with special reference to the deposits of high-density turbidity currents. Journal of Sedimentary Petrology 52, 279–297.

Malkowski, M.A., Grove, M., Graham, S.A., 2015. Unzipping the Patagonian Andes—long-lived influence of rifting history on foreland basin evolution. Lithosphere 8, 23–28. http://dx.doi.org/10.1130/L489.1.

Maslin, M., Vilela, C., Mikkelsen, N., Grootes, P., 2005. Causes of catastrophic sediment failures of the Amazon Fan. Quaternary Science Reviews 24, 2180–2193. http://dx.doi.org/10.1016/j.quascirev.2005.01.016.

McHargue, T., Pyrcz, M.J., Sullivan, M.D., Clark, J.D., Fildani, a., Romans, B.W., Covault, J.A., Levy, M., Posamentier, H.W., Drinkwater, N.J., 2011. Architecture of turbidite channel systems on the continental slope: patterns and predictions. Marine and Petroleum Geology 28, 728–743. http://dx.doi.org/10.1016/j.marpetgeo.2010.07.008.

Moretti, I., Calassou, S., Victor, P., Molinaro, M., Maerten, L., 2003. Syn-Sedimentary shear zones. Petroleum Geoscience 9, 221–232.

Morley, C.K., 2003. Mobile shale related deformation in large deltas developed on passive and active margins. Geological Society of London, Special Publication 216, 335–357.

Morley, C.K., 2015. Mobile Shale Related Deformation in Large Deltas Developed on Passive and Active Margins. pp. 335–357.

Morley, C.K., Guerin, G., 1996. Comparison of gravity-driven deformation styles. Tectonics 15, 1154–1170.

Moscardelli, L., Wood, L., 2008. New classification system for mass transport complexes in offshore Trinidad. Basin Research 20, 73–98. http://dx.doi.org/10.1111/j.1365-2117.2007.00340.x.

Moscardelli, L., Wood, L., 2015. Morphometry of mass-transport deposits as a predictive tool. Bulletin Geological Society of America 128, 47–80. http://dx.doi.org/10.1130/B31221.1.

Moscardelli, L., Wood, L., Mann, P., 2006. Mass-transport complexes and associated processes in the offshore area of Trinidad and Venezuela. American Association of Petroleum Geologists Bulletin 90, 1059–1088. http://dx.doi.org/10.1306/02210605052.

Mulder, T., Alexander, J.A.N., 2001. The physical character of subaqueous sedimentary density flows and Their deposits. Sedimentology 48, 269–299.

Mutti, E., Sonnino, M., 1981. Compensation cycles: a diagnostic feature of turbidite sandstone lobes. Int. Ass. Sed. 2nd European Meeting, Bologna, Abstracts, pp. 120–123.

Nardin, T.R., Hein, F.J., Gorsline, D.S., Edwards, B.D., 1979. A review of mass movement processes sediment and acoustic characteristics, and contrasts in slope and base-of-slope systems versus canyon-fan-basin floor systems. SEPM Special Publication 27, 61–73.

Olafiranye, K., Jackson, C.A.-L., Hodgson, D.M., 2013. The role of tectonics and mass-transport complex emplacement on upper slope stratigraphic evolution: a 3D seismic case study from offshore Angola. Marine and Petroleum Geology 44, 196–216. http://dx.doi.org/10.1016/j.marpetgeo.2013.02.016.

Patton, T.L., 2005. Sandbox models of downward-steepening normal faults. American Association of Petroleum Geologists Bulletin 89, 781–797.

Perret, D., Locat, J., Leroueil, S., 1995. Strength development with burial in fine-grained sediments from the Saguenay fjord, Quebec. Canadian Geotechnical Journal 32, 247–262.

Prélat, A., Hodgson, D.M., 2013. The full range of turbidite bed thickness patterns in submarine lobes: controls and implications. Journal of the Geological Society of London 170, 209–214.

Prélat, A., Hodgson, D.M., Flint, S.S., 2009. Evolution, architecture and hierarchy of distributary deep-water deposits: a high-resolution outcrop investigation from the Permian Karoo Basin, South Africa. Sedimentology 56, 2132–2154. http://dx.doi.org/10.1111/j.1365-3091.2009.01073.x.

Prélat, A., Covault, J.A., Hodgson, D.M., Fildani, A., Flint, S.S., 2010. Intrinsic controls on the range of volumes, morphologies, and dimensions of submarine lobes. Sedimentary Geology 232, 66–76. http://dx.doi.org/10.1016/j.sedgeo.2010.09.010.

Romans, B.W., Hubbard, S.M., Graham, S.A., 2009. Stratigraphic evolution of an outcropping continental slope system, Tres Pasos Formation at Cerro Divisadero, Chile. Sedimentology 56, 737–764. http://dx.doi.org/10.1111/j.1365-3091.2008.00995.x.

Romans, B.W., Fildani, A., Graham, S.A., Hubbard, S.M., Covault, J.A., 2010. Importance of predecessor basin history on sedimentary fill of a retroarc foreland basin: provenance analysis of the Cretaceous Magallanes basin, Chile (50–52°S). Basin Research 22, 640–658. http://dx.doi.org/10.1111/j.1365-2117.2009.00443.x.

Romans, B.W., Fildani, A., Hubbard, S.M., Covault, J.A., Fosdick, J.C., Graham, S.A., 2011. Evolution of deep-water stratigraphic architecture, Magallanes Basin, Chile. Marine and Petroleum Geology 28, 612–628. http://dx.doi.org/10.1016/j.marpetgeo.2010.05.002.

Schwartz, T.M., Graham, S.A., 2015. Stratigraphic architecture of a tide-influenced shelf-edge delta, Upper Cretaceous Dorotea Formation, Magallanes-Austral Basin, Patagonia. Sedimentology 62, 1039–1077. http://dx.doi.org/10.1111/sed.12176.

Sharman, G.R., Graham, S.A., Masalimova, L.U., Shumaker, L.E., King, P.R., 2015. Spatial patterns of deformation and paleoslope estimation within the marginal and central portions of a basin-floor mass-transport deposit, Taranaki Basin, New Zealand. Geosphere 11, 266–306. http://dx.doi.org/10.1130/GES01126.1.

Shultz, M.R., Hubbard, S.M., 2005. Sedimentology, stratigraphic architecture, and ichnology of gravity-flow deposits partially ponded in a growth-fault-controlled slope minibasin, Tres Pasos Formation (Cretaceous), southern Chile. Journal of Sedimentary Research 75, 440–453. http://dx.doi.org/10.2110/jsr.2005.034.

Shultz, M.R., Fildani, A., Cope, T.D., Graham, S.A., 2005. Deposition and stratigraphic architecture of an outcropping ancient slope system: Tres Pasos Formation, Magallanes Basin, southern Chile. Geological Society of London, Special Publication 244, 27–50.

Straub, K.M., Pyles, D.R., 2012. Quantifying the hierarchical organization of compensation in submarine fans using surface statistics. Journal of Sedimentary Research 82, 889–898. http://dx.doi.org/10.2110/jsr.2012.73.

Sultan, N., Voisset, M., Marsset, B., Marsset, T., Cauquil, E., Colliat, J.L., 2007. Potential role of compressional structures in generating submarine slope failures in the Niger Delta. Marine Geology 237, 169–190. http://dx.doi.org/10.1016/j.margeo.2006.11.002.

Talling, P.J., Masson, D.G., Sumner, E.J., Malgesini, G., 2012. Subaqueous sediment density flows: Depositional processes and deposit types 1937–2003. http://dx.doi.org/10.1111/j.1365-3091.2012.01353.x.

van der Merwe, W.C., Hodgson, D.M., Flint, S.S., 2009. Widespread syn-sedimentary deformation on a muddy deep-water basin-floor: the vischkuil formation (Permian), Karoo Basin, South Africa. Basin Research 21, 389–406. http://dx.doi.org/10.1111/j.1365-2117.2009.00396.x.

Vendeville, B.C., 2005. Salt tectonics driven by sediment progradation: part I - mechanics and kinematics. American Association of Petroleum Geologists Bulletin 89, 1071–1079.

Waldron, J.W.F., Gagnon, J., 2011. Recognizing soft-sediment structures in deformed rocks of orogens. Journal of Structural Geology 33, 271–279. http://dx.doi.org/10.1016/j.jsg.2010.06.015.

Williams, E., 1960. Intra-stratal flow and convolute folding. Geological Magazine 97, 208–214 (http://dx.doi.org.ezproxy.lib.vt.edu/10.1017/S0016756800061380).

Wilson, T.J., 1991. Transition from back-arc to foreland basin development in the southernmost Andes: stratigraphic record from the Ultima Esperanza District, Chile. GSA Bulletin 103, 98–111.

Winn, R.D.J., Dott, R.H.J., 1977. Large-scale traction-produced structures in deep-water fan-channel conglomerates in southern Chile. Geology 5, 41–44.

Xiao, H., Suppe, J., 1992. Origin of Rollover. American Association of Petroleum Geologists Bulletin 76, 509–520.